Soft Matter

Accepted Manuscript

ROYAL SOCIETY OF CHEMISTRY

www.rsc.org/softmatter

ARTICLE TYPE www. rsc.org/xxxxxx | XXXXXXXX

Statistical analysis of vesicle morphology dynamics based on free energy landscape†

Soichiro Tsuda,[a] Hiroaki Suzuki,[b,c] and Tetsuya Yomo*[c,d,e]

Received Xth XXXXXXXXXX 20XX, Accepted Xth XXXXXXXXX 20XX
First published on the web Xth XXXXXXXXXX 200X
DOI: 10.1039/b000000x

We here present a method to reconstruct effective free energy landscapes (FELs) of lipid vesicles from statistical analysis of a large number of microscope images. This method, not just allows us to define possible energy landscapes, but also highlights minority vesicle shapes that were otherwise hidden in the majority. When compared with temporal evolutions of deforming lipid vesicles, it was found that the trajectory of deforming vesicles was in accordance with the reconstructed landscape, in which the minority shapes play a key role. When compared with theoretical models, it revealed that the vesicle shapes characterised in the reconstructed FELs were consistent with the theoretically predicted shapes. These results suggest that the FEL analysis can be a useful tool to investigate the morphological dynamics of lipid vesicles, in conjunction with other analytical methods.

1 Introduction

Lipid vesicles have been long serving as simplified models of biological cell to elucidate the physicochemical basis of biological structure and function[1,2] as well as to construct "protocells", cell-like systems encapsulating a minimal set of biological molecules.[3–5]

The structural simplicity of lipid vesicles render them the ideal model systems to study theoretically and experimentally to understand how the membrane dynamics contributes to cellular activities, such as exo/endocytosis and lipid raft formation.[6] A number of experiments were so far carried out on the shape changes of vesicles upon various external stimulations, such as temperature change,[7] osmotic pressure,[8] and pore-forming peptides.[9] Recently, we found that giant vesicles containing polymer molecules exhibit spontaneous budding transformations when they are fused.[10]

In practice, these shape transformation behaviours of giant vesicles are often analysed by tracking changes of giant vesicle shapes upon external stimulation under the microscope. While this method provides us direct evidences, quantitatively estimating statistical properties of vesicle behaviours (*e.g.* the effect of an external stimulus) can be complicated due to the morphological diversity of vesicles. Even with vesicles in a single preparation, a wide range of shape transformations can often arise in response to the stimulus.[7,11]

This vesicle heterogeneity is theoretically due to the extreme softness of lipid bilayers with respect to bending[12], and experimentally caused by various reasons, such as slight differences in bilayer asymmetry among vesicles, metastability and hysterisis of vesicle shapes.[13] This could make it difficult to obtain a statistically-significant number of samples showing similar behaviour, especially when the shape transformations of interest are rare.

To circumvent this issue, we here propose a statistical approach to capture the shape transformation dynamics of lipid vesicles: Instead of tracking temporal variations of a small number of vesicles, snapshots of a large number of vesicles at a single time point are employed for analysis. An effective free energy landscape (effective FEL) is reconstructed from frequency distributions of vesicle shapes, which should be inversely proportional to energy levels.

The FEL reconstruction method is often employed to study protein folding dynamics.[14–16] In those methods, principal component analysis (PCA) plays a crucial role to extract a few appropriate coordinates which well represent the protein dynamics among many other coordinates. PCA is a well-established mathematical method for mapping high-

[a] *School of Chemistry, University of Glasgow, Glasgow, G12 8QQ, Scotland, UK.*
[b] *Department of Precision Mechanics, Chuo University, 1-13-27 Kasuga, Bunkyo-ku, Tokyo 112-8551, Japan.*
[c] *Yomo Dynamical Micro-scale Reaction Environment Project, ERATO, Japan Science and Technology Agency, 1-5 Yamadaoka, Suita, Osaka, 565-0871, Japan.*
[d] *Graduate School of Information Science and Technology, Osaka University, 1-5 Yamadaoka, Suita, Osaka, 565-0871, Japan*
[e] *Graduate School of Frontier Biosciences, Osaka University, 1-5 Yamadaoka, Suita, Osaka, 565-0871, Japan. FAX: +81 (0)6 6879 7433; TEL: +81 (0)6 6879 4151; E-mail: yomo@ist.osaka-u.ac.jp*
† Electronic Supplementary Information (ESI) available: Detailed descriptions of shape-characterising indexes, reconstruction of FEL in one dimensional case, calculation of theoretical vesicle shapes using spherical harmonics parameterisation method, and the minimum bending energy at reduced volume $v = 0.63$, Comparison of different shape-characterising indexes, examples of vesicle shapes in FEL space, and distribution of parameter values. See DOI: 10.1039/b000000x/

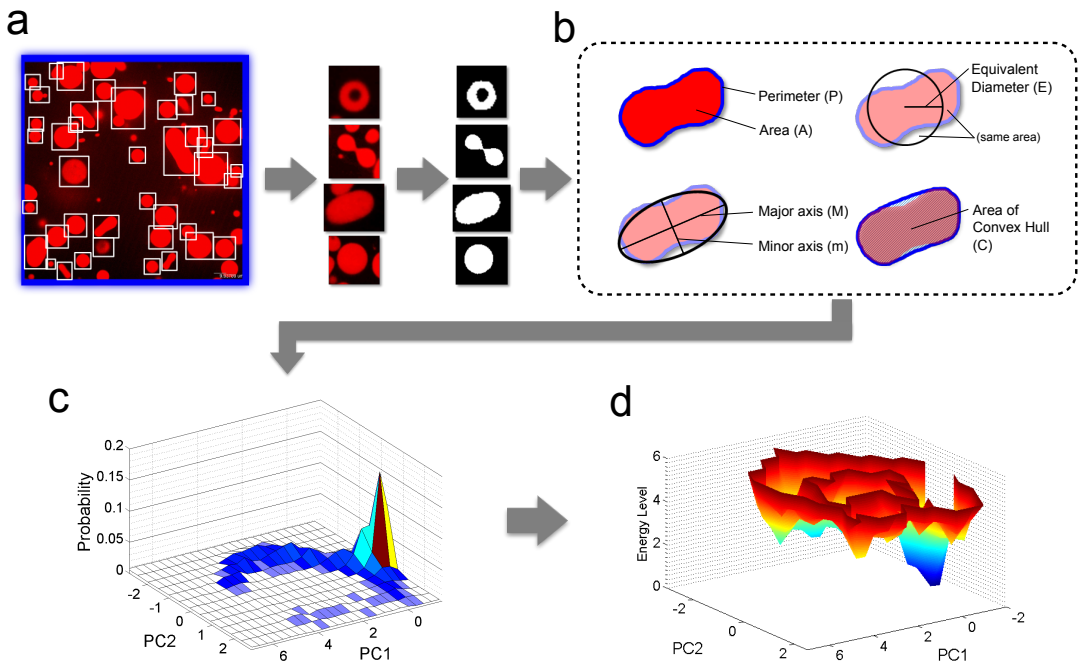

Fig. 1 A schematic diagram of FEL reconstruction process. (a) Vesicle image analysis for binarisation. (b) Measure shape properties of vesicles to quantify each vesicle image as multi-dimensional data. (c) Calculate the probabilities (frequency distributions) by reducing the quantified data into one or two-dimenions using PCA. (d) Construct an "effective FEL" by taking a negative logarithm of (c).

dimensional data onto lower dimensions, while maintaining variations in the original data set. Thus, a first few principal components are expected to represent characteristic structures in the high-dimensional data. In our case, PCA is employed to obtain a set of new coordinates among multiple shape-characterising measures. As we deal with a population of lipid vesicles, which can include a variety of shapes such as stomatocyte, oblate, and pear-like shape, a single measure may not be suitable for characterising shapes.

The construction of FEL has been attempted mostly in theoretical models of vesicles including continuum elastic theory,[17] triangulated-surface model,[18,19] and coarse-grained molecular dynamics,[20,21] in which parameters for vesicle shapes can be conveniently varied. A pioneering work of reconstructing a FEL from experimental data is done by Döbereiner and Seifert.[22] They analysed time series images of a single vesicle shape (contour) and mapped an effective FEL from frequency distribution data of the vesicle contours.

In contrast to the previous research, we here take a method to reconstruct a FEL of lipid vesicles from statistical frequency distributions of vesicle shapes, similar to the method used for protein dynamics research. Figure 1 summarises the reconstruction process: First, vesicle images are cropped from original images taken by a confocal scanning microscope and then binarised for quantification (Fig. 1a). Several shape properties are extracted to quantify and characterize each vesicle shape (Fig. 1b). This multi-dimensional shape data are reduced to one or two-dimenion using principal component analysis (PCA) and the probabilities (frequency distributions) are calculated (Fig. 1c). The free energy, defined as a negative logarithm of the probability distributions, are calculated to construct effective FELs (Fig. 1d).

This paper is organised as follows: First, we applied the FEL reconstruction method to statistically investigate the effect of osmotic pressure on the vesicle shapes. By comparing FELs at different osmotic conditions (section 3.1), we could extract characteristic vesicle shapes at each condition. Second, we mapped a sequence of temporally deforming vesicles onto a FEL to compare the statistical and temporal dynamics of vesicle shape transformation. We found that the temporal evolution of vesicle deformation shows a similar trend to the reconstructed FEL (section 3.2). Lastly, we discussed reconstructed FELs in relation to a theoretical model of vesicle shapes in section 4.

2 Materials and methods

2.1 Materials

1-palmitoyl-2-oleoyl-*sn*-glycero-3-phosphocholine (POPC) and 1-palmitoyl-2-oleoyl-*sn*-glycero-3-[phospho-*rac*-(1-

glycerol)] (POPG) were purchased from Avanti Polar Lipids (Alabaster, USA), and cholesterol was purchased from Nacalai Tesque (Kyoto, Japan). These lipids were dissolved in chloroform and stored in a freezer at -20 °C to avoid any degradation of lipids. Fluorescent protein, transferrin from human serum Alexa Fluor®647 conjugate (TA647) was purchased from Invitrogen (Carlsbad, USA).

Aqueous solution encapsulated in giant vesicles (hereafter referred to as "inner solution") contains 50 mM HEPES-KOH (pH 7.6), 200 mM sucrose, and 2 μM TA647. Buffer solution contains 50 mM HEPES-KOH (pH 7.6), 200 mM glucose (hereafter, "outer solution"). Hypertonic buffer solutions contain 50 mM HEPES-KOH (pH 7.6) with different concentrations of glucose higher than 200 mM.

2.2 Preparation of Giant Unilamellar Vesicles

For statistical analysis of lipid vesicles, we need to prepare a homogeneous initial population. The water-in-oil (W/O) emulsion method[4,23,24] was thus employed to prepare lipid veiscles. In our previous work, we found that this method can reliably produce unilamellar and spherical vesicles, while vesicles produced by other methods tend to create multilamellar vesicles, often with inner structure (smaller vesicles inside) and the shapes are not spherical due to the multilamellarity.[25] Lamellarity was confirmed by FACS analysis in the previous literature[25] and sphericity was checked by confocal microscopy. Thus, a population of vesicles prepared by the W/O emulsion method can be assumed to be homogeneous in terms of bending regidity (i.e. unilamellar) and shape (most vesicles are spherical and the reduced volume is close to 1).

Vesicle formation by this method comprises two main steps: (1) Formation of W/O emulsion droplets in liquid paraffin containing lipids and (2) formation of unilamellar vesicles by centrifugation. Briefly, the mixture of POPC, POPG, and cholesterol in chloroform at weight ratio of 9:1:0.5 was dissolved in liquid paraffin, and chloroform was evaporated in the oven at 80 °C for at least 20 min. The final concentration of lipids in liquid paraffin was 5 mg/mL. Fifty microlitres of the inner solution was added to 500 mL lipid/paraffin solution and vortexed thoroughly for 30 s to form W/O emulsions. The mixture was kept on ice for 10 min so that lipids assemble at the water-oil intrface. It was then transferred gently on top of 400 μL outer solution. By centrifuging at 4 °C, 18,000 g for 30 min, emulsions in liquid paraffin form unilamellar vesicles when they pass through the interface between oil and water. Further details can be found elsewhere.[25]

2.3 Microscope Observation

We have carried out two types of microscope observations, using a laser scanning confocal microscope (IX71, Olympus, Japan) and differential interference constrast (DIC) microscope (Eclipse Ti-U, Nikon, Japan).

The confocal microscope was used to obtain fluorescent snapshot images of vesicles with clear and sharp contours, which make subsequent image analysis easier. Prior to the observation, a hypertonic buffer solution was gently added to an outer solution containing vesicles in order to make a desired hypertonic condition of outer solution. We tested four osmotic conditions: 200, 240, 280, and 320 mM of glucose in the outer solution. We refer to these conditions as 200, 240, 280, and 320 mM conditions, respectively. The mixture was settled at least for 1 h on a glass slide to equlibrate the vesicle shapes deformed by osmotic stress. Vesicles sink down to the bottom of the glass slide due to the the sugar asymmetry across the vesicle membrane. Thus the major axis of vesicles under observation should be in parallel with the XY plane of the microscope. During the observation, a stack of images along Z-axis was taken at each XY position.

The DIC microscope was used to observe shape changes of vesicles for long periods of time without photobleaching. Vesicles were exposed to hypertonic conditions as described above, but within 5 min they were observed under the microscope to capture spontaneous shape transformations of vesicles. Sequential images of vesicles at a fixed XYZ position were taken for several minutes to over an hour.

2.4 Analysis of Vesicle Images

Obtained images were first binarised to extract contours of vesicles. For fluorescence confocal microscope images, a Z plane that maximises the diameter of each vesicle is manually chosen first, then binarised using adaptive histogram equalization algorithm on Matlab (Fig. 1a). Vesicles smaller than 5 μm or larger than 20 μm in diameter were omitted from analyses. In total, 1600 vesicles are used to analyse for each osmotic condition.

Once images are binarised, following properties are measured for each vesicle (Fig. 1b): Area (denoted as A), perimeter (P), major/minor axes (M and m, the longest and shortest diameters of an approximated ellipsoid), equivalent diameter (E, the diameter of a circle with the same area as the vesicle), and area of convex hull (C, area of the smallest convex polygon that covers the vesicle).

Based on these geometrical properties, following non-dimensional measures for characterising vesicle shapes are defined (hereafter, "shape-characterising indexes". See ESI S-1 for detailed descriptions):

(1) Elongation (EL) $\equiv \log_2(M/m)$
(2) Distorsion (DS) $\equiv A/Pm$
(3) Eccentricity (EC) $\equiv \sqrt{1-m^2/M^2}$
(4) Solidity (SL) $\equiv A/C$

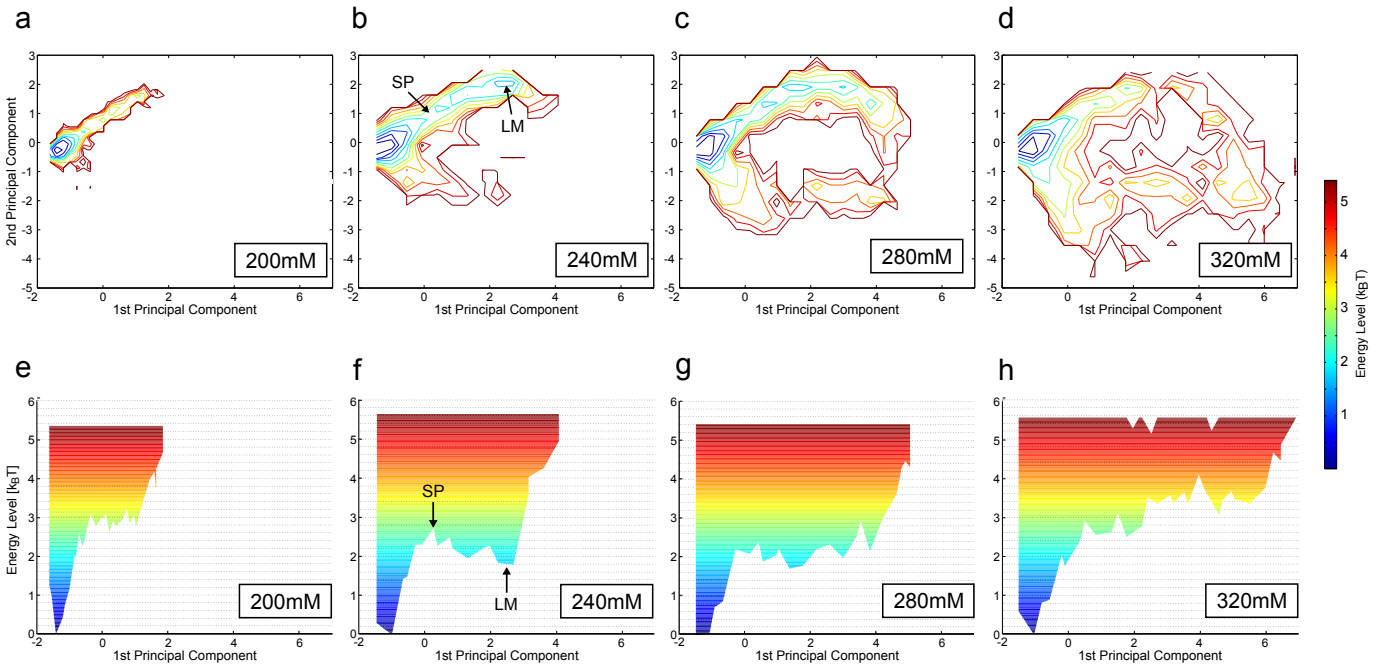

Fig. 2 The reconstructed FELs for the 200, 240, 280 and 320 mM conditions viewed from the top (a-d) and viewed from the side (e-h). In the FEL of the 240 mM condition (b and f), a local minimum (LM) and a saddle point (SP) between global and local minima are shown.

(5) Roundness Factor (RNF) $\equiv P/E$

The choice of these indexes are basically arbitrary. However, (1) they are the measures commonly used for image analysis to numerically describe morphology of particles, including powders, crystals and emulsions.[26–28] And (2) The parameters are defined to be dimensionless so that the size of vesicles does not affect the analysis. We adopted dimensionless parameters because, with dimensional parameters, we found that one of the first two principal components always corresponded to the size. In order to have more separated distributions in the reconstructed FEL, we empirically adopted dimensionless measures for our analysis so that we can distinguish different shapes in FELs. See ESI S-1 for further details of the indexes and ESI S-5 for comparison of PCA plots using different shape-characterising indexes.

2.5 Principal Component Analysis

PCA takes a $p \times n$ matrix, $\mathbf{q}$, with p being variables (i.e. shape-characterising indexes) and n the number of samples (vesicles being analysed). This matrix was first standardised for each variable as as $q = (q - \langle q \rangle)/\sigma$, where $q \in \mathbf{q}$ and σ is a standard deviation of samples. Eigenvectors $\mathbf{W}$ and eigenvalues λ of a covariance matrix $\mathbf{C} = \langle (\mathbf{q} - \langle \mathbf{q} \rangle)(\mathbf{q} - \langle \mathbf{q} \rangle)^T \rangle$ are calculated from the standardised $\mathbf{q}$. Principal components $\mathbf{z}$ are defined as $\mathbf{z} = \mathbf{W}\mathbf{q}$, in which the i-th principal component z_i is represented as:

$$z_i = \sum_{j=1}^{p} w_{ij} q_j \tag{1}$$

where $w_{ij} \in \mathbf{W}, q_j \in \mathbf{q}$ $(i, j = 1, \cdots, p)$ are a component weight and a value of each shape-characterising index of a vesicle, respectively. Hereafter, principal components are abbreviated as PC1, PC2, and so on.

In practice, samples of all the osmotic conditions are combined to make a large $\mathbf{q}$ and then the principal components are calculated for $\mathbf{q}$. By this operation, a location in the reconstructed FEL always corresponds to a specific vesicle shape regardless of the osmotic conditions (cf. Fig. 3), which make comparisons between FELs straightforward.

2.6 Free Energy Landscape

The free energy landscape of vesicle shape transformation can be obtained from principal components. A principal component was separated into 30 statistical bins for each dimension and the probability for each bin, $P(s)$, is defined as the number of samples in the bin divided by the total samples. A free energy F for a region is defined as:

$$F = -k_B T \ln \frac{P(s)}{P_{max}(s)} \tag{2}$$

where k_B is the Boltzmann constant, T is the temperature, and $P_{max}(s)$ is the maximum probability in all the regions. A FEL

was obtained by mapping F along principal components.

3 Results

3.1 Reconstruction of FEL: 2D case

We reconstructed FELs using the first two principal components to further look into the effect of osmotic pressure on the shape deformation (For 1D case, see ESI S-2). Figure 2 shows reconstructed FELs for the 200, 240, 280 and 320 mM conditions viewed from top and side, respectively (cf. Fig. 1d for 3D view). At 200 mM isotonic condition (Fig. 2a and e), the FEL has only one global minimum around at (PC1, PC2) = (-1.35, 0). When the external osmotic condition became hypertonic at 240 mM, the reconstructed FEL expanded to the upper right and lower right directions (Fig. 2b) and a region around at (PC1, PC2) = (2.5, 2) forms a local minimum (indicated as LM in Fig. 2b and f), which is connected to the global minimum via a saddle point (SP in Fig. 2b and f). The region remained to be a local minimum at the 280 mM condition too (Fig. 2c and g). In contrast, a small "island" in Fig. 2b at (PC1, PC2) = (2, -1.5) became larger and the overall FEL takes a ring-like shape. At the even more hypertonic 320 mM condition, the local minimum region shrunk drastically, while smaller islands appear in the right half of the FEL (Fig. 2d and h).

A lower energy region in the reconstructed FELs indicates that lipid vesicles of a specific shape exist relatively more than other shapes. This is because vesicles characterised by the shape-characterising indexes are expected to be mapped onto a similar location in a FEL, and FELs are constructed based on the frequency distributions of vesicle shapes defined in eq. (2). This means it is possible to correlate a location in a FEL and a vesicle shape.

To confirm this, we checked mappings between FEL locations and original vesicle images. Typical images corresponding to characteristic locations are shown in Fig. 3. The global minimum indicated as blue contour in all the FELs corresponds to a circular shape (Fig. 3 type 1). In fact, at the 200 mM isotonic condition, most of observed vesicle shapes were shpherical and the corresponding FEL showed a single-well profile. Type 2-4 shapes correspond to prolate shapes. In particular, vesicles in type 3 shape form a local minimum in the FELs of 240 and 280 mM condition, whereas type 2 shape forms a saddle point. This indicates type 3 shape is a more stable in these osmotic conditions (i.e. more frequently observed in the microscope observation), compared to type 2 shape. Type 5 shapes are stomatocytes, in which internal cavity is represented as a black spot inside a vesicle in the image. Asymmetric or symmetric bowling pin-like vesicles are type 6 and 7. They are relatively minority shapes compared to the other shapes. Type 7 shapes were observed only in the 320 mM condition.

Note that the shapes except Fig. 3 type 1 were rather "minority" shapes when observed under the microscope and many of observed vesicle shapes were circular (hence the global minimum). Those minor shapes were highlighted by taking the logarithm of frequencies in eq. (2). For example, a raw frequency distribution of 2D PCA in Fig. 1c has only one sharp peak corresponding to the circular vesicles, while the FEL in Fig. 1d has multiple wells of various vesicles including circular ones.

Above results show that the FEL reconstruction analysis can successfully categorise various vesicle shapes. In fact, a region in the FEL always consisted of vesicles with similar shapes and there was no region with mixed shapes (See ESI S-6). ESI S-7 shows the raw parameter values are almost randomly distributed in the FELs and also show how the shape-characterisation index are distributed.

The FELs visualised what kind of vesicle shapes can be observed when they are exposed to different osmotic conditions. What was crucial here was the logarithm in eq. (2). By taking a negative log, the reconstructed FELs highlight minority vesicle shapes, such as prolates and stomatocytes, which were otherwise hidden in the majority if we simply performed a statistical analysis.

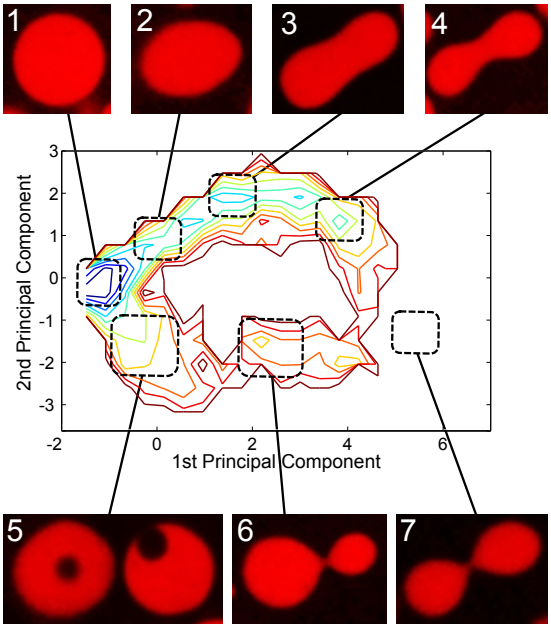

Fig. 3 The mapping between locations in the FEL and vesicle shapes. Note that the FEL of 280 mM condition is shown for illustration purpose only and the vesicle images were taken from various osmotic conditions to show as a map. The mapping between them was always the same regardless of the osmotic condition (cf. section 2.5).

3.2 Mapping temporal vesicle transformation onto the reconstructed FEL

In the previous subsections, we have obtained effective FELs, which were based on statistical data. In this section, we investigate the relationship between the reconstructed FELs and temporally deforming vesicles by mapping the temporal trajectories onto the FEL. By comparing the statistical and temporal data, we would be able to know if the FELs reflect temporal dynamics of vesicle shape transformations.

Experiments were carried out as follows: Lipid vesicles were exposed to a hypertonic condition as with the previous experiments. After being settled for 5 min, they were observed under the microscope at 10fps. A few out of over hundreds of vesicles in the field of view exhibited spontaneous shape transformations in this condition. Sequential DIC images of vesicles at a fixed XYZ position were taken for analysis. Each recorded snapshot was analysed as in section 2.4 and mapped onto a FEL by calculating PC1 and PC2 using the weights w_{ij} obtained in eq. (1).

Figure 4 shows some image frames of an observed shape change under the 240 mM condition and the corresponding trajectory mapped onto the reconstructed FEL. A commonly observed transformation proceeded as follows (see Supplementary Movie): A vesicle that was initially spherical developed into a stomatocyte shape with one or more cavities (Fig. 4a). The cavities suddenly disappeared at some point (Fig. 4b), followed by a sequence of characteristic shape transformation (Fig. 4c-f). The vesicle first transformed to into an axisymmetric oblate shape (Fig. 4c). Although we did not have any Z-axis information for this, we speculated the shape was oblate because (1) it was unlikely that a sudden volume change (e.g. influx of water into the vesicle) occurred in such a short period, but (2) the diameter of the vesicle suddenly increased by approximately 20 % between Fig. 4b and c. It then quickly changed to a axisymmetric prolate (Fig. 4e) via an intermediate non-axisymmetric oblate shape (Fig. 4d). After the vesicle remained in the prolate shape for a while, it formed a daughter vesicle by an asymmetric budding (Fig. 4f).

Figure 4g represents a trajectory of a vesicle transformation mapped onto the reconstructed FEL of 240 mM condition. As described above, the vesicle was initially moving around at the global minium region. It then migrated to the local minium (prolate) through the saddle point. It should be noted that the trajectory of the vesicle at the saddle point region (indicated as "d") was unidirectional, whereas that at the global/local minima appeared to be rather stochastic. Accordingly, the vesicle passed through the saddle point region quickly (approximately in 11 s in this case), whereas it stayed in the local minimum for a longer period (approximately 47 s). This result suggests that the reconstructed FEL from statistical data do reflect the temporal transformation dynamics of lipid vesciles.

On the other hand, it also illustrates a problem: spherical vesicles and disc-like oblates are both mapped in a similar location in the FEL. This is because they are indistinguishable in 2D microscope images. This explains why the vesicle in Fig. 4 moved away from the global minimum to local minima: disc-like oblates are generally at higher energy states than prolates (cf. Fig. 5b and c) and hence went through the shape transformations. In this sense, the global minimum is a superposition of a true global minimum of spherical vesicles and a local minimum of oblates. The only way to distinguish these shapes is to include the height information of vesicles. In order to improve the FEL reconstruction, 3D information (i.e. the thickness of vesicles) would need to be incorporated in the future analysis.

All the observed budding transformation in the condition exhibited similar time developments as above. In particular, the transformation from oblate to prolate (Fig. 4c to e) always completed in a short period. It has been also observed that vesicles stopped transformations either in oblate or prolate and remained stable in the shape afterwards.

While the budding transformation was commonly observed in the 240 mM condition, we did not observe similar transformations in other conditions. In the 280 mM and 320 mM conditions, there were three types of shape changes with stomatocytes: (1) They remained stable in the shape throughout the observation, (2) slowly transformed into oblate shape and remained stable, or (3) burst immediately after cavities disappeared. We discuss possible reasons why vesicles at these conditions are not showing budding transformations in section 4.2.

4 Discussion

In an attempt to further look into the reconstructed effective FELs, we here compare the FELs with predictions from a theoretical vesicle model.

So far there are a number of theoretical models proposed to explain the vesicle shapes. Among others, the curvature-based models are often used to model actual vesicle shapes that are experimentally obsered, such as Spontaneous Curvature (SC) model,[29] Bilayer Couple (BC) model,[30] and Area-to-Difference Elasticity (ADE) model.[13] Those models all assume that vesicle shapes were achieved by minimising the bending energy of bilayer membrane, but differ in physical constants and parameters.[17] In general, the ADE model is considered as a more general model and the BC models is one of extreme cases of the ADE model, in which assumes deviations of the area difference ΔA and the equilibrated area difference ΔA_0 are always equal. We here employs the BC model because the shape deformations observed here appeared to be continuous (i.e. second-order transition) as they gradually transform

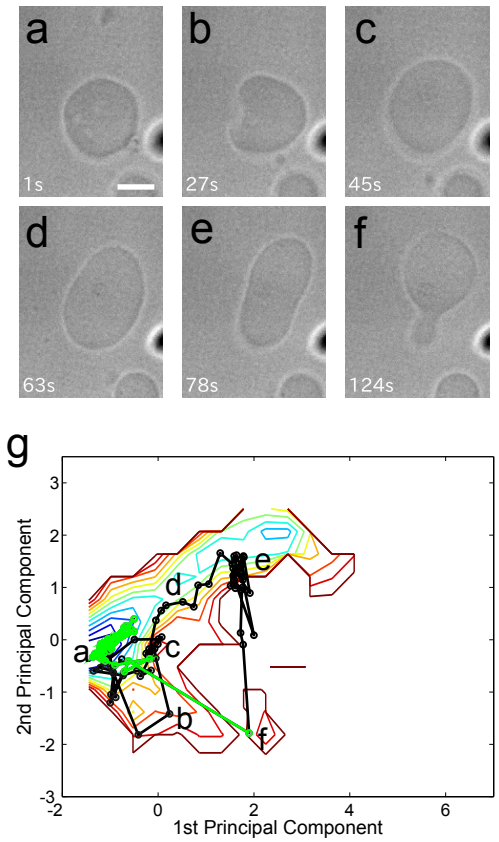

Fig. 4 (a-f) Snapshots of a budding vesicle under the DIC microscope. Numbers in the lower left indicate time and a scale bar in (a) is 10μm. (g) A trajectory of the vesicle shape transformation (black) mapped onto the reconstructed FEL for the 240 mM condition. Alphabets in the plot indicate locations of (a-f) vesicles. After the completion of budding, a trajectory for a mother vesicle was plotted as green for visualisation.

from, for exmple, an oblate shape to prolate. In this sense, the BC model seems to be more suitable to describe the transition.

The BC model employs a bending energy function to calculate vesicle shapes:

$$W_b/8\pi\kappa_b = \frac{1}{2}\oint (C_1+C_2)^2 dA \qquad (3)$$

where κ_b is the bending ridigity, C_1, C_2 local mean curvatures, and A the total surface area.

The BC model determines a vesicle shape under two constraints, (1) reduced volume $v = V/(4\pi/3){R_A}^3$, where V is the enclosed volume and $R_A = \sqrt{A/4\pi}$, and (2) reduced area difference $\Delta a = M/4\pi{R_A}^2$, where $M = 1/2\oint(C_1+C_2)dA$. A vesicle shape is calculated as a shape with the minimum W_b that satisfies the v and Δa constraints. To calculate the minimum energy shapes, a method that numerically solves Euler-Lagrange equations has been conventionally employed.[30] Here we use the spherical harmonics parameterisation (SHP) method.[32] This method, in contrast to the conventional one, does not assume axisymmetry for the shape calculation (see ESI S-3 for more details). Note that, the results obtained by the SHP method are same as the conventional method because both models employ the same bending enery functions and a shape under a set of constraints is detemined through the energy minimisation process. What is different is the way to compute the minimum energy shapes. The SHP method allows us to readily compute non-axisymmetric shapes as well as axisymmetric ones. Comparisons of the SHP method with other methods can be found elsewhere.[32] We employed this method because it allows us to easily compute the non-axisymmetric minimum energy shapes as well as axisymmetric ones in the same theoretical framework and compare them with shapes observed in previous sectioins.

4.1 Stable shapes in different osmotic conditions

In section 3.1, we have observed that prolate shapes formed a local minimum at the 240 mM and 280 mM conditions (Fig. 2b and Fig. 3). This would suggest that prolate shapes are favoured in the 240 and 280 mM conditions. To check this observation, we calculated bending energies of typical vesicle shapes (prolate, oblate and stomatocyte) for each osmotic condition.

In theory, a vesicle encapsulating 200 mM sucrose solution will equilibrate in the 240 mM glucose outer solution if it is shrunk to 83 % of the original volume (For simplicity, we ignored the osmotic contribution from fluorescent protein). Thus, the tested osmotic conditions, 200, 240, 280, and 320 mM conditions, correspond to the reduced volume $v = 1$, 0.83, 0.71, and 0.63, respectively, in terms of the BC model.

Figure 5a shows a plot of bending energies of the three shapes against the reduced volume calculated using the SHP model. Prolate shapes are energetically preferred for $0.65 < v < 1$, whereas oblate shapes are for $0.59 < v < 0.65$. For the region smaller than $v = 0.59$, stomatocyte, which bending energy is always $W_b = 2$, is energetically favoured. It should be noted that this result is exactly same as the previous literature calculated using the Lagrange multiplier method[30] and proves the validity of using the SHP model to discuss theoretical predictions of vesicle shapes.

When compared to the experimental results, this is consistent with the results that prolate shapes formed local minima in the FELs of 240 mM ($v = 0.83$) and 280 mM ($v = 0.71$) conditions, which indicate that the prolate shapes are relatively stable in the conditions. In addition, the local minimum of prolate shapes disappeared at the 320 mM condition ($v = 0.63$) in Fig. 2c and f. In this region, oblates are the-

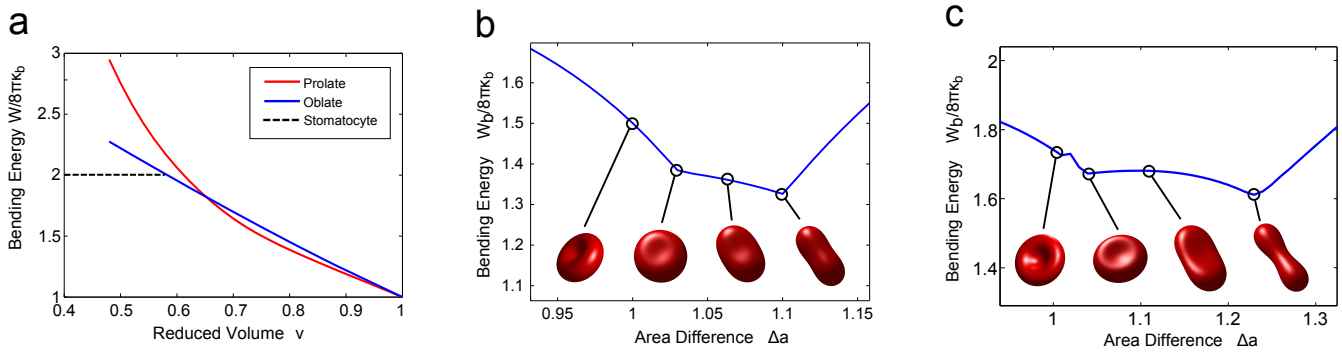

Fig. 5 (a) A plot of bending energies W_b for prolate and oblate shapes as a function of reduced volume v. (b) A plot of the minimum bending energy W_b against area difference Δa for $v = 0.83$. Four typical shapes are shown in the plot: stomatocyte, axisymmetric oblate, non-axisymmetric oblate, and axisymmetric prolate (left to right), which area differences are $\Delta a = 1.0, 1.03, 1.06, 1.1$, respectively. (c) A plot of the minimum bending energy W_b for $v = 0.83$. Area differences for the shapes are $\Delta a = 1.0, 1.04, 1.11, 1.23$, respectively.

oretically expected to have lower bending energies than prolates (Fig. 5a). Although we were not able to compare oblate shapes in the FEL with those from the theoretical model due to the technical limitation described above, we observed that vesicle shapes are dominantly stomatocytes at higher osmotic conditions, e.g. 400 mM condition ($v = 0.5$, data not shown). This partly supports that the results from FEL analysis show good agreement with theoretical predictions of vesicle shapes.

4.2 Vesicle shapes with various area differences

Next, we compared predicted vesicle shapes of the BC model with experimentally observed shapes at each osmotic condition.

Figure 5b shows a plot of the bending energy as a function of the area difference Δa at $v = 0.83$ (equivalent to the 240 mM condition). Typical predicted shapes were stomatocyte shape ($\Delta a = 1.0$), axisymmetric oblate ($\Delta a = 1.03$), non-axisymmetric oblate ($\Delta a = 1.06$), and axisymmetric prolate ($\Delta a = 1.1$), which were also found in in the FEL (see Fig. 2b and Fig. 3 type 1,2,3 and 5). It is noteworthy that there is a strong resemblance between the axisymmetric prolate, which has the smallest bending energy at this reduced volume, and the shape of vesicle that forms a local minimum (LM) in Fig. 2b (Fig. 3 type 3). In addition, these predicted shapes look similar to a series of the transforming vesicle shapes in Fig. 4a-f. It can be seen from Fig. 5b that the shape transformation from the stomatocyte to prolate observed in Fig. 4 was actually an energy relaxation process.

This also suggests that the transformation into budding shape involve an 'apparent' change in area difference Δa between the bilayer membranes. In fact, similar behaviour was also reported recently by Sakashita et al.[31] They observed osmotially-induced shape transformations of vesicles and found that vesicles exhibited the increase of decrease in Δa upon spontaneous transformation. As lipid vesicles used here, POPC and POPG, are known to show very slow flip-flop[33], other factors may have contributed to the change in Δa, such as the flip-flop of cholesterol to relax the bending energy[34] or sub-microscopic lipid reservoirs which have been formed in the process of vesicle formation.[35]

Figure 5c shows a plot of the bending energy at $v = 0.71$. The vesicle shapes predicted at this condition are also analogous to those found in the FEL of 280 mM condition: For example, a similar shape of an axisymmetric prolate can be found in Fig. 3 (type 4). The stomatocyte shape ($\Delta a = 1.0$) has a larger and deeper cavity compared to the one with the same Δa at $v = 0.83$. When this is mapped onto the FEL, it corresponds to the expanded stomatocyte region (lower right of Fig. 3 type 5 region): In the confocal microscope image, a stomatocyte is shown as a circle with a black spot. As stomatocytes with larger cavity (larger black spot) are mapped onto a lower right region, stomatocytes predicted at $v = 0.71$ correspond to the expanded region in the FEL of 280 mM condition. Shapes at $v = 0.63$ also predicted similar shapes fouund in the 320 mM condition (see ESI, S-4).

Although shapes found at these conditions were similar to the ones at $v = 0.83$, they have larger Δa gaps between shapes: For example, at $v = 0.83$, stomatocyte ($\Delta a = 1.0$) and axisymmetric prolate ($\Delta a = 1.1$) have 0.1 difference in Δa, whereas they have 0.23 difference at $v = 0.71$ ($\Delta a = 1.0$ and 1.23, respectively). This means that a transformation from one shape to another at $v = 0.71$ requires a larger change in area difference than at at $v = 0.83$. We speculate that this would explain the shape transformation behaviour in section 3.2. It has been observed the budding transformation was observed only at the 240 mM condition, while at the other conditions a characteristic shape change was a transformation from stomatocyte to oblate only. When compared to the shapes in Fig. 5b and c, it can be seen that both transformations involve a change in

Δa of roughly 0.1 units. This would suggest that lipid vesicles in these osmotic conditions allow 10 % change in terms of area difference. Considering that shape transformations of lipid vesicles are very sensitive to bilayer asymmetry,[36] this flexible nature of lipid membranes help vesicles achieve various shapes, which might have helped primitive living organisms (protocells) dynamically react to changing environments too.

5 Conclusions

In conclusion, we have presented a method to characterise lipid vesicle shapes in terms of free energy landscape using statistical microscopic data. It has been observed that a temporally deforming vesicle showed transformation behaviour in accordance with the reconstructed landscape. Comparisons with theoretical vesicle shapes showed that the characteristic vesicle shapes in the reconstructed FELs were consistent with theoretical predictions.

Over more than three decades, a number of experimental studies were carried out that discuss in relation to theoretical models. To our best knowledge, The FEL method to characterise lipid vesicle shapes using microscopic data is the first research on the statistical analysis of lipid vesicle shapes, while previous studies mainly focused on the temporal transformations. What was really critical in the FEL analysis we think was the logarithm in eq. (2): By taking a logarithm of probability distributions, it highlights minority vesicle shapes that were otherwise hidden in the majority, which would be difficult to find just with statistical analysis. In addition, the flexiblity of lipid membrane was estimated through the FEL analysis in conjunction with the temporal analysis and theoretical prediction of vesicle shapes.

This method can be easily applied to shape transformation experiments induced by other external stimuli, such as temperature and pH change. We believe that it can be used as a useful tool to investigate the morphological dynamics of lipid vesicles, in conjunction with other analytical methods.

Acknowledgements

Authors would like to thanks Dr Khaled Khairy for his help on theoretical modeling of vesicles, and Dr Kazuya Nishimura for technical suggestions on vesicle experiments. This work is partly supported by Grant-in-Aid for Young Scientists (B) No. 24740290 from Japan Society for the Promotion of Science (JSPS).

References

1 *The Minimal Cell: The Biophysics of Cell Compartment and the Origin of Cell Functionality*, ed. P. Luisi, Pier Luigi; Stano, Springer, 2011.
2 V. Weissig, *Liposomes: Methods and Protocols, Volume 2: Biological Membrane Models*, Humana Press, 2010.
3 H. Kita, T. Matsuura, T. Sunami, K. Hosoda, N. Ichihashi, K. Tsukada, I. Urabe and T. Yomo, *ChemBioChem*, 2008, **9**, 2403–10.
4 V. Noireaux, Y. T. Maeda and A. Libchaber, *Proc. Natl. Acad. Sci. USA*, 2011, **108**, 3473–80.
5 T. Nishikawa, T. Sunami, T. Matsuura, N. Ichihashi and T. Yomo, *Anal. Chem.*, 2012, 5017–5024.
6 T. Baumgart, G. Hunt, E. R. Farkas, W. W. Webb and G. W. Feigenson, *Biochim. Biophys. Acta*, 2007, **1768**, 2182–2194.
7 J. Käs and E. Sackmann, *Biophys. J.*, 1991, **60**, 825–44.
8 H. G. Döbereiner, J. Käs, D. Noppl, I. Sprenger and E. Sackmann, *Biophys. J.*, 1993, **65**, 1396–403.
9 Y. Yu, J. A. Vroman, S. C. Bae and S. Granick, *J. Am. Chem. Soc.*, 2010, **132**, 195–201.
10 H. Terasawa, K. Nishimura, H. Suzuki, T. Matsuura and T. Yomo, *Proc. Natl. Acad. Sci. USA*, 2012, **109**, 5942–5947.
11 M. Yanagisawa, M. Imai, T. Taniguchi and F. Ade, *Phys. Rev. Lett.*, 2008, **100**, 1–4.
12 U. Seifert and R. Lipowsky, *Structure and Dynamics of Membranes: From Cells to Vesicles*, Elsevier, 1995, vol. 1, ch. 8, pp. 403–463.
13 L. Miao, U. Seifert, M. Wortis and H.-G. Döbereiner, *Phys. Rev. E*, 1994, **49**, 5389–5407.
14 N. Panahi and R. Berry, *Phys. Chem. Chem. Phys.*, 2009, **11**, 11638–11646.
15 G. G. Maisuradze, A. Liwo and H. A. Scheraga, *J. Mol. Biol.*, 2009, **385**, 312–329.
16 G. Maisuradze, A. Liwo and H. Scheraga, *Phys. Rev. Lett.*, 2009, **102**, 1–4.
17 U. Seifert, *Adv. Phys.*, 1997, **46**, 13–137.
18 H. Noguchi and G. Gompper, *Phys. Rev. E*, 2005, **72**, 011901.
19 S. J. Zhao and J. T. Kindt, *Europhys. Lett.*, 2007, **69**, 839–845.
20 W. Shinoda, T. Nakamura and S. O. Nielsen, *Soft Matter*, 2011, 9012–9020.
21 C. Guo, Y. Luo, R. Zhou and G. Wei, *ACS Nano*, 2012, **6**, 3907–3918.
22 H.-G. Döbereiner and U. Seifert, *Europhys. Lett.*, 1996, **36**, 325.
23 S. Pautot, B. J. Frisken and D. a. Weitz, *Langmuir*, 2003, **19**, 2870–2879.
24 S. Pautot, B. J. Frisken and D. a. Weitz, *Proc. Natl. Acad. Sci. USA*, 2003, **100**, 10718–10721.
25 K. Nishimura, T. Hosoi, T. Sunami, T. Toyota, M. Fujinami, K. Oguma, T. Matsuura, H. Suzuki and T. Yomo, *Langmuir*, 2009, **25**, 10439–10443.
26 T. Tomita, T. Sugawara and Y. Wakamoto, *Langmuir*, 2011, **27**, 10106–10112.
27 J. D. M.-N. Pons, H. Vivier, *Part. Part. Svst. Charact.*, 1997, **14**, 272–277.
28 V. Mikli, H. Käerdi, P. Kulu, and M. Besterci, *Proc. Est. Acad. Sci. Eng.*, 2001, **7**, 22–34.
29 W. Helfrich, *Z. für Naturforschung*, 1973, **28**, 693–703.
30 S. Svetina and B. Zeks, *Eur. Biophys. J.*, 1989, **17**, 101–111.
31 A. Sakashita, N. Urakami, P. Ziherl and M. Imai, *Soft Matter*, 2012, **8**, 8569–8581.
32 K. Khairy and J. Howard, *Soft Matter*, 2011, **7**, 2138.
33 M. Nakano, M. Fukuda, T. Kudo, N. Matsuzaki, T. Azuma, K. Sekine, H. Endo and T. Handa, *The Journal of Physical Chemistry B*, 2009, **113**, 6745–6748.
34 R. J. Bruckner, S. S. Mansy, A. Ricardo, L. Mahadevan and J. W. Szostak, *Biophys. J.*, 2009, **97**, 3113–3122.
35 R. Bar-Ziv, E. Moses and P. Nelson, *Biophysical Journal*, 1998, **75**, 294–320.
36 K. Berndl, J. Käs, R. Lipowsky, E. Sackmann and U. Seifert, *Europhys. Lett.*, 1990, **13**, 659–664.

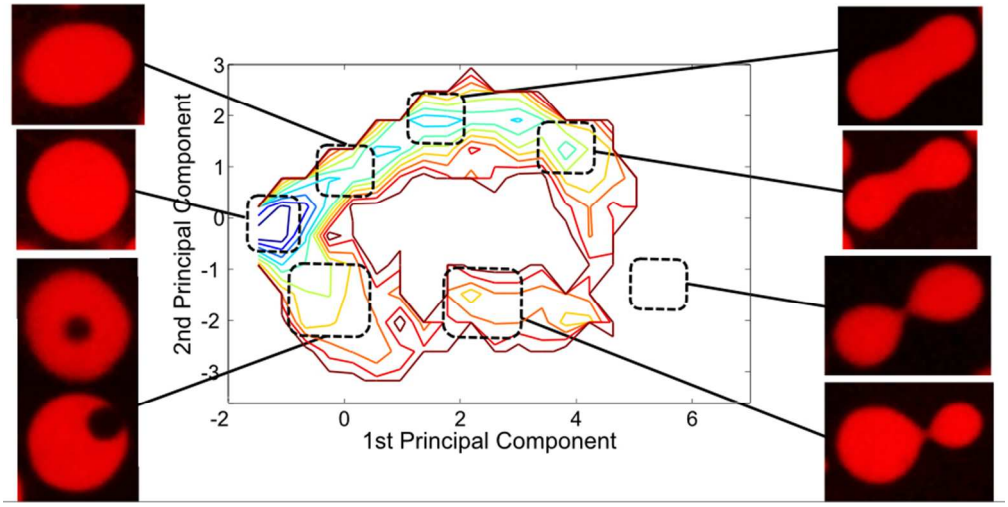

We here present a method to reconstruct effective free energy landscapes (FELs) of lipid vesicles from statistical analysis of a large number of microscope images.
80x39mm (300 x 300 DPI)